

Journal of Geophysical Research: Planets

RESEARCH ARTICLE

10.1029/2018JE005752

Key Points:

- Juno crossed flux tubes connected to Io's footprint tail aurora 10° to 120° downstream of the main Alfvén wing (MAW) spot
- Broad power law-like electron energy distributions suggest a primarily broadband acceleration mechanism
- Juno observed structure with ~20-km resolution, bifurcated tails, and broadening with longitudinal separation from the MAW spot

Correspondence to:

J. R. Szalay,
jszalay@princeton.edu

Citation:









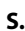











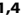

Szalay, J. R., Bonfond, B., Allegrini, F., Bagenal, F., Bolton, S., Clark, G., et al. (2018). In situ observations connected to the Io footprint tail aurora. *Journal of Geophysical Research: Planets*, 123. <https://doi.org/10.1029/2018JE005752>

Received 6 JUL 2018

Accepted 3 OCT 2018

Accepted article online 10 OCT 2018

In Situ Observations Connected to the Io Footprint Tail Aurora

J. R. Szalay^{1,2} , B. Bonfond³ , F. Allegrini^{1,4} , F. Bagenal⁵ , S. Bolton¹ , G. Clark⁶ , J. E. P. Connerney^{7,8} , R. W. Ebert¹ , R. E. Ergun⁵ , G. R. Gladstone¹ , D. Grodent³ , G. B. Hospodarsky⁹ , V. Hue¹ , W. S. Kurth⁹ , S. Kotsiaros⁸ , S. M. Levin¹⁰ , P. Louarn¹¹ , B. Mauk⁶ , D. J. McComas^{2,1} , J. Saur¹² , P. W. Valek^{1,4} , and R. J. Wilson⁵ 

¹Southwest Research Institute, San Antonio, TX, USA, ²Department of Astrophysical Sciences, Princeton University, Princeton, NJ, USA, ³Space Sciences, Technologies and Astrophysics Research Institute, LPAP, Université de Liège, Belgium, ⁴Department of Physics and Astronomy, University of Texas at San Antonio, San Antonio, TX, USA, ⁵Laboratory for Atmospheric and Space Physics, University of Colorado Boulder, Boulder, CO, USA, ⁶The Johns Hopkins University Applied Physics Laboratory, Laurel, MD, USA, ⁷Space Research Corporation, Annapolis, MD, USA, ⁸Goddard Space Flight Center, Greenbelt, MD, USA, ⁹Department of Physics and Astronomy, University of Iowa, City, IA, USA, ¹⁰Jet Propulsion Laboratory, Pasadena, CA, USA, ¹¹Institut de Recherche en Astrophysique et Planétologie, Toulouse, France, ¹²Institute of Geophysics and Meteorology, University of Cologne, Cologne, Germany

Abstract The Juno spacecraft crossed flux tubes connected to the Io footprint tail at low Jovian altitudes on multiple occasions. The transits covered longitudinal separations of approximately 10° to 120° along the footprint tail. Juno's suite of magnetospheric instruments acquired detailed measurements of the Io footprint tail. Juno observed planetward electron energy fluxes of ~70 mW/m² near the Io footprint and ~10 mW/m² farther down the tail, along with correlated, intense electric and magnetic wave signatures, which also decreased down the tail. All observed electron distributions were broad in energy, suggesting a dominantly broadband acceleration process, and did not show any broad inverted-V structure that would be indicative of acceleration by a quasi-static, discrete, parallel potential. Observed waves were primarily below the proton cyclotron frequency, yet identification of a definitive wave mode is elusive. Beyond 40° down the footprint tail, Juno observed depleted upward loss cones, suggesting that the broadband acceleration occurred at distances beyond Juno's transit distance of 1.3 to 1.7 R_J. For all transits, Juno observed fine structure on scales of approximately tens of kilometers and confirmed independently with electron and wave measurements that a bifurcated tail can intermittently exist.

Plain Language Summary The Juno spacecraft crossed regions magnetically connected to auroral structures associated with Jupiter's moon Io on multiple occasions. The transits covered longitudinal separations of approximately 10° to 120° along Io's auroral tail. Juno's suite of instruments acquired detailed measurements of these auroral structures. Juno directly observed the electrons that sustain these auroral features before they crash into the atmosphere and generate the brilliant aurora. The flux of these electrons decreased as Juno transited the tail farther from Io's longitude. While there are two main explanations for Io's auroral signatures, the nature of the observed electrons in this work favors one mechanism over the other. When Juno was far from Io's longitude, the observations suggest that the spacecraft was below the point at which the electrons are accelerated into the atmosphere. For all transits, Juno observed fine structure on scales of approximately tens of kilometers and confirmed that a bifurcated tail can intermittently exist.

1. Introduction

Jupiter's intense aurora provides a window into the complex magnetosphere-ionosphere coupling that exists throughout its vast magnetosphere (Bagenal et al., 2014). There are many distinct features in the Jovian aurora (e.g., reviewed by Grodent, 2015), which are typically categorized into the oval-shaped main auroral emission, diffuse emissions equatorward of the main oval, polar emissions, and the Galilean satellite footprint spots and tails. Of the many Jovian auroral features, Jupiter's innermost Galilean satellite, Io, generates one of the most consistent and identifiable aurorae, both in the infrared (Connerney et al., 1993; Connerney & Satoh, 2000) and ultraviolet (Clarke et al., 1996).

Unlike the other auroral features, whose source locations are unclear due to uncertainties in magnetic field mapping and time variations, the footprints of the Galilean moons provide an unambiguous origin of the

magnetospheric source for these phenomena. Io's auroral signature has a rich morphology, including (1) the main Alfvén wing (MAW) spot (Bonfond et al., 2008; Saur et al., 2013) that is directly related to Io's immediate interaction with the corotating plasma, (2) a transhemispheric electron beam spot that is suggested to be a conjugate aurora related to the MAW, (3) a reflected Alfvén wing spot from reflections within the Io torus, and (4) the long auroral tail trailing the Io footprint in the ionosphere. Throughout this paper, we use the term *Io footprint tail* (IFPT) to describe the auroral tail trailing (downstream of) the MAW, and it is this IFPT that is the focus of our study.

Since the 1960s Io has been known to trigger bursts of radio emission (Bigg, 1964; Goldreich & Lynden-Bell, 1969; reviewed by Zarka, 1998). The 1979 Voyager 1 flyby of Io showed magnetic and flow perturbations (Acuna et al., 1981; Belcher et al., 1981) consistent with an Alfvénic disturbance being generated by the corotating plasma moving past the moon (Neubauer, 1980). These Alfvén waves travel to Jupiter along the magnetic field, reflect off the strong density gradient in the ionosphere, and bounce between hemispheres (Bagenal, 1983; Gurnett & Goertz, 1981; Jacobsen et al., 2007). Electrons are clearly accelerated in the process because they bombard the atmosphere and produce hydrogen emissions associated with Io. But the process whereby the electrons are accelerated remains unclear.

Two distinct mechanisms have been proposed to produce the electrons responsible for the aurora associated with Io. One mechanism, here referred to as *quasi-static*, suggests that the MAW spot and the IFPT are sustained by two separate processes, with the MAW spot being generated by the Alfvénic interaction of the plasma with Io's atmosphere (e.g., Neubauer, 1998; Saur et al., 2013) and the IFPT being sustained by a quasi-steady current system set up to transfer angular momentum from Jupiter to the subcorotating Io-genic plasma downstream from Io (Delamere et al., 2003; Ergun et al., 2009; Hill & Vasyliunas, 2002; Matsuda et al., 2012; Su et al., 2003). A direct consequence of such a current system would be the existence of large quasi-static parallel potentials, on the order of 1–70 keV (given in the previous references, where more recent results indicate the lower potential of ~1 keV), which would accelerate electrons into the Jovian ionosphere. The other explanation, here referred to as *purely Alfvénic*, is that the various spots and the IFPT are all generated by the same Alfvénic acceleration mechanism, with the tail being sustained by multiple reflections of Alfvén waves between the Io torus and the ionosphere (Bonfond et al., 2009; Bonfond, Saur, et al., 2017; Cray & Bagenal, 1997; Jacobsen et al., 2007, 2010). These two separate mechanisms should produce identifiably distinct signatures in any plasma instrument taking high-latitude measurements at Jupiter. In the quasi-static parallel potential scheme, an electron instrument would be expected to see inverted-V structures and peaked intensities at the predicted acceleration energies of 1–70 keV. On the other hand, a purely Alfvénic acceleration process would lead to power law-like electron distributions, with no discernible peak in the intensity spectra. Additionally, bidirectional electron fluxes are predicted to exist within the Alfvénic acceleration region at high latitudes due to field aligned, oscillating electric fields (Hess et al., 2010; Jones & Su, 2008). Determining the existence and location of this acceleration region has remained an open issue, as some studies suggest the Alfvénic acceleration occurs primarily inside the Io torus (Crary, 1997; Das & Ip, 1992).

Close to Io, the Galileo spacecraft observed strongly bidirectional field-aligned electron beams with power law electron distributions over plasma (0.2 to 8 keV) and energetic particle (15–150 keV) energy ranges in the regions over the poles of Io and within the near-Io wake (Frank & Paterson, 1999; Williams et al., 1996; Williams & Thorne, 2003). It was concluded that the acceleration of these beams occurs at low Jovian altitudes, given the ~6° beam widths, and that the plasma component contained sufficient energy flux to yield measureable auroral emissions. However, the most reasonable interpretation of these beams, based on analogy with Earth auroral processes, is that Galileo was observing the upward acceleration (with respect to Jupiter) associated with the downward component of the Io interaction electric circuit (Mauk et al., 2001; Williams & Thorne, 2003). It was considered unlikely that Galileo was observing the electrons directly causing the Io-associated auroral emissions. Specifically, if a quasi-static parallel acceleration were responsible for the emissions, the evidence for that could only be observed far away from Io itself, near the quasi-static acceleration region should one exist.

In this study, we will use data from four instruments aboard the Juno mission: (1) JADE, the Jovian Auroral Distributions Experiment (McComas, Alexander, et al., 2017); (2) the Waves instrument (Kurth, Hospodarsky, et al., 2017); (3) the Magnetometer (Connerney et al., 2017); and (4) UVS, the Ultraviolet Spectrograph (Gladstone et al., 2017). We note that the JADE instrument is well suited to study the IFPT plasma

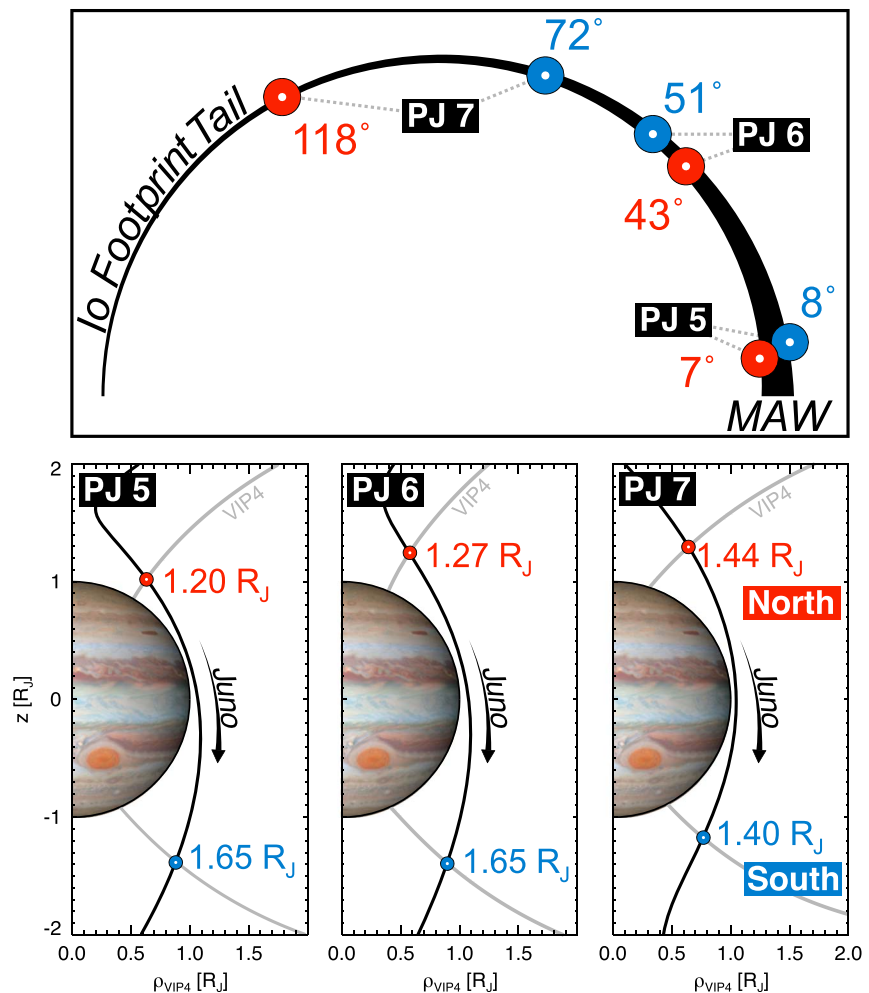


Figure 1. (top) A schematic view of the Io footprint tail from above the north pole and the positions of Juno (circles) during the footprint tail connected measurements for the northern (red) and southern (blue) passes. (bottom, left) PJ5, (middle) PJ6, and (right) PJ7 show the Juno trajectory in the dipole magnetic frame, with +z aligned with the VIP4 magnetic dipole moment. The trajectory shown is $\rho_{VIP4} = \sqrt{x^2 + y^2}$ in these coordinates. MAW = main Alfvén wing; PJ = perijove.

structures as it measures electron fluxes in the range of 0.1–100 keV, which spans the energy range of 1–70 keV for the predicted parallel potentials. JADE has already enabled investigations of Jupiter’s magnetosheath and outer magnetosphere during Juno’s approach (Ebert et al., 2017a; Gershman et al., 2017; McComas, Szalay, et al., 2017), observed a hot flow anomaly upstream of Jupiter (Valek et al., 2017), and made the first close-in polar measurements of low-energy ion and electron populations (Allegrini et al., 2017; Ebert et al., 2017b; Louarn et al., 2017; Szalay et al., 2017). Here we report on the measurements taken when JADE observed enhanced electron fluxes connected to the Io tail as well as measurements from all previously listed Juno instruments. In section 2, we describe relevant details about the orbit geometry. Section 3 addresses the specific details of each instrument’s measurements. We conclude in section 4 with a discussion on the implications of these measurements in the context of our continually evolving view of Jovian auroral structures.

2. Orbit Geometry

The bottom row in Figure 1 shows the flyby geometry in a frame aligned with the dipole approximation to Jupiter’s VIP4 magnetic field model. The term *M* shell is used in lieu of *L* shell to distinguish that we are not using a dipolar magnetic field model to map field lines from Jupiter to the magnetosphere; we primarily use VIP4 (Connerney et al., 1998), a magnetic field model constrained by the Io’s flux tube footprint, in this

study for consistency with Juno data comparisons. In these figures, the gray magnetic field lines show the M shells (VIP4) for the specific short-duration Io tail events discussed in this work. The Juno orbit is precessing southward, such that its apojove is farther south on each successive orbit. Due to the evolution of Juno's trajectory and relative phase of Jupiter's dipole, Juno typically transits $M = 6 R_J$ flux tubes at closer planetocentric distances in the north, with correspondingly larger velocities. The top panel of Figure 1 shows a schematic view of the IFPT from above the north pole and the positions of Juno (circles) during the footprint tail connected measurements for the northern (red) and southern (blue) passes, using VIP4 as well.

Figure 2 shows the radiance observations from UVS in System III coordinates for the northern and southern hemispheres. The footprint of the Juno trajectory using the VIP4 (Connerney et al., 1998) and VIPAL (Hess et al., 2011) internal field models is shown with the red and green lines, respectively, determined by tracing magnetic field lines to the 1-bar level at Jupiter. Both use an explicit model of the magnetodisk (Connerney et al., 1981) to approximate the external magnetospheric magnetic field. VIPAL employs an additional constraint accounting for Io's longitudinal position (Hess et al., 2011). We show both VIP4 and VIPAL on the UVS images in this work as these have been widely used in previous literature (e.g., Vogt et al., 2015). Yellow lines indicate the direction of the Sun from the beginning to end of the observations and white dots show hourly tick marks. Gray dashed lines show constant Jovian longitudes and latitudes. The south pole images are displayed as viewed from above the north pole down through Jupiter. The IFP and IFPT can be clearly seen in most images, in close proximity to the average Hubble Space Telescope (HST) Io footprint location shown with the dot-dashed white oval (Bonfond, Saur, et al., 2017). These images show how Juno transited the Io tail over a broad range of longitudinal separations with the MAW. The discrepancy between the predicted MAW at the time of the crossing (red cross) and MAW spot location on the UVS images is due to the time offset and averaging needed to create a reasonably complete snapshot of the Jovian aurora, particularly since UVS does not observe the MAW when Juno actually transits the Io tail aurora. The measurement periods are given in the time labels at the top right of image.

3. Measurements

In this section, we detail the specific measurements from each instrument. The JADE instrument provides the primary plasma measurements relevant to the specific acceleration mechanism sustaining the IFPT. Waves observations provide context to the plasma measurements by constraining the wave modes encountered by the Juno spacecraft. Lastly, UVS provides direct imaging of the auroral structures and provides additional context for the particles and field observations. Table 1, as discussed throughout this section, lists the properties of the Io footprint signatures in the different instruments for northern and southern passes on PJ5, PJ6, and PJ7, as will be discussed in the following subsections.

3.1. JADE Electron Measurements for 0.1–100 keV

JADE consists of two separate subsystems, JADE-E that measures electrons and JADE-I that measures ions (McComas, Alexander, et al., 2017). In this study, we focus on the electron measurements. JADE-E consists of two separate, nearly identical top-hat analyzers capable of detecting incident electrons over the energy range of 0.1–100 keV. Each sensor has a field of view of 120° in azimuth by 2 – 5.5° in elevation. The two sensors combined have 240° azimuthal coverage. They can also electrostatically deflect up to 35° above and below Juno's spin plane to track the magnetic field direction. JADE-E measures the full (180°) pitch angle (PA) distribution for one third of the spin (10 s out of 30 s at 2 rpm) and more than two thirds ($>120^\circ$ of 180°) of the PA distribution for the remaining two thirds of the spin.

When Juno is very near to Jupiter, JADE-E is put into its high-rate science mode, with 1-s temporal resolution. For the perijoves (PJ) discussed in this study, Juno transits flux tubes connected to the Io torus (M shell $\approx 6 R_J$) at 45–55 km/s relative to Jupiter, such that it can resolve structures on the order of 50 km along the Juno velocity vector for each 1-s measurement.

Building upon previous analyses, the JADE data help discriminate between different magnetospheric environments connected along B to the Juno spacecraft (Szalay et al., 2017). While JADE was connected to regions interior to the Io torus (M shells of ~ 3 – $6 R_J$), both JADE-E and JADE-I experienced large amounts of penetrating radiation, with no evidence of any discernible plasma structures. Once connected to the Io torus, JADE-I

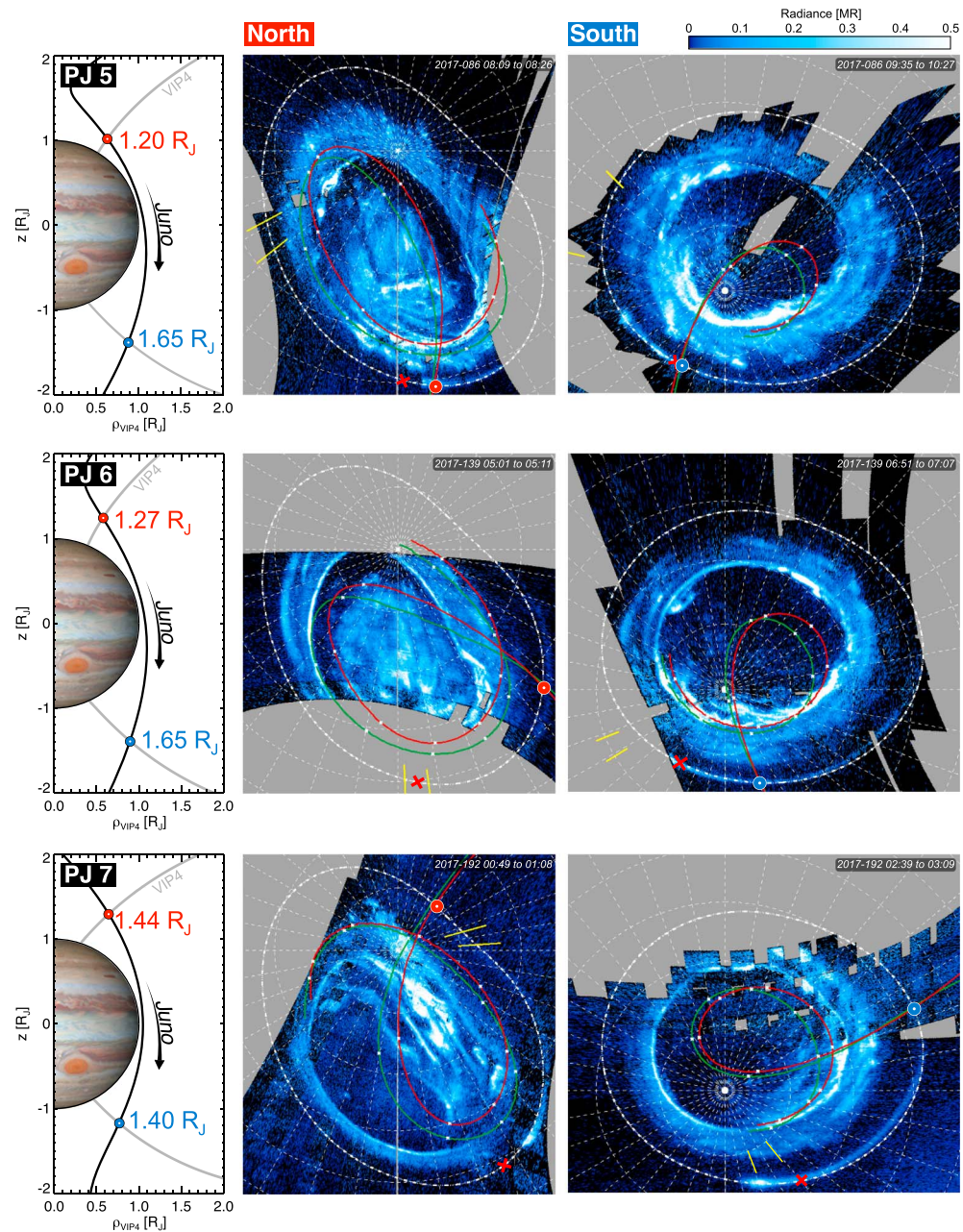


Figure 2. Rows correspond to (top) PJ5, (middle) PJ6, and (bottom) PJ7. (left column) See Figure 1 description. (middle and right columns) Ultraviolet Spectrograph images taken during both perijoves for the northern and southern hemispheres. The white dot-dashed oval line shows the average Hubble Space Telescope Io footprint (Bonfond, Saur, et al., 2017). Red crosses show the predicted Io main Alfvén wing spot, and the circles show the Juno's intersection with the Io footprint tail. The green and red lines show the Juno orbit mapped to the Jovian surface using VIPAL and VIP4, respectively, with the white dots shown every UTC hour. Yellow lines show the longitude range of the solar direction during each observation window. PJ = perijove.

measures magnetospheric H^+ and heavy ions. However, these regions (M shells of $\sim 6\text{--}8 R_J$) lack electrons within JADE-E's energy range, presumably due to the Io torus electron temperature: too cold to appreciably populate field lines well above the equator, where Juno transits these M shells. While this does not preclude the possibility of electron fluxes below the current noise level (in the high penetrating radiation environment in this region), JADE-E typically observed significant electron populations over 100 eV once connected to $M > 8 R_J$ (Allegrini et al., 2017; Szalay et al., 2017).

Table 1
Parameters for the IFPT Flux Tube Crossings During PJ5–PJ7

DOY	PJ5				PJ6				PJ7			
	2017–086				2017–139				2017–192			
Time (UTC)	08:34:36	08:34:42	09:30:51	09:31:02	05:39:28	05:39:41	06:39:54	06:40:03	01:24:39	01:25:00	02:22:27	02:22:54
R	1.198 R_J	1.196 R_J	1.643 R_J	1.648 R_J	1.268 R_J	1.264 R_J	1.647 R_J	1.651 R_J	1.448 R_J	1.440 R_J	1.391 R_J	1.400 R_J
θ_{VIP4}	57.69°	57.50°	−57.75°	−57.95°	59.10°	58.76°	−57.95°	−58.10°	63.59°	63.11°	−56.32°	−56.93°
θ_{III}	51.73°	51.52°	−64.66°	−64.86°	60.24°	59.85°	−63.77°	−63.93	74.93°	74.47°	−48.21°	−48.87°
Local time	16:53		16:38		16:42		16:17		16:45		16:05	
$\Delta\lambda_{Io}$ (VIP4)	7°		8°		43°		51°		118°		72°	
$\Delta\theta_{Jup}$ (VIP4)	0.17°		0.18°		0.33°		0.15°		0.41°		0.61°	
θ_{Io} (VIP4)	9.4°		9.0°		9.1°		9.3°		4.5°		7.8°	
θ_{Io} (Cen _{VIP4})	6.3°		6.0°		6.1°		6.2°		3.0°		5.2°	
w_{Jup}	210 ± 34 km		220 ± 20 km		390 ± 30 km		180 ± 20 km		470 ± 23 km		720 ± 27 km	
w_{sc}	320 ± 54 km		510 ± 46 km		680 ± 52 km		410 ± 46 km		1030 ± 49 km		1350 ± 50 km	
ΔM (VIP4)	6.6 R_{Io}		3.7 R_{Io}		5.4 R_{Io}		3.3 R_{Io}		9.4 R_{Io}		9.0 R_{Io}	
$\langle B \rangle$	7.4 G		1.7 G		4.5 G		1.7 G		2.2 G		2.5 G	
$ \delta B_{\perp max} $	25 nT		6.25 nT		25 nT		6.25 nT		12.5 nT		12.5 nT	
$F_{E,max}$	72 mW/m ²		14 mW/m ²		7 mW/m ²		8 mW/m ²		17 mW/m ²		7 mW/m ²	

Note. Red/blue columns indicate northern/southern hemispheres, respectively. The distance w_{sc} is calculated as $v_{sc}\Delta t$. Errors are given for ± 1 s from the boundaries. DOY = day of year; PJ = perijove; IFPT = Io footprint tail.

During PJ1, PJ3, and PJ4, Juno's footprint on Jupiter was never closer than $\sim 220^\circ$ longitude to the MAW, and JADE did not measure significant fluxes associated with the various components of Io's footprint. During PJ5, PJ6, and PJ7, Juno's footprint intersected the Io tail flux tubes with predicted Juno-MAW angular separating from $\sim 10^\circ$ to 120° (Table 1; $\Delta\lambda_{Io}$ calculated using the VIP4 model).

For each of these close approaches (PJ5–PJ7), during the times Juno was expected to be connected to the most interior regions of the Io torus and verified by inspection of JADE-I H^+ data, JADE measured large enhancements in both upward and downward electron fluxes. Figure 3 shows these JADE electron measurements, in differential energy flux (DEF) and PA. Waves measurements are also shown alongside these electron measurements, as will be discussed in section 3.2. Note that upward/downward refers to the direction with respect to the planet. Upward fluxes correspond to PAs of 0° in the northern hemisphere and 180° in the southern hemisphere, relative to the magnetic field that is directed out of Jupiter's north and into the south pole. Each PA bin is 7.5° wide, consistent with the JADE-E individual anode angular resolution (see Allegrini et al., 2017; McComas, Alexander, et al., 2017, for a more complete description of the PA determination). The gap in electron azimuthal detection coverage leads to a periodic gap in PA coverage, which is shown as the black portions in the PA spectrograms. Due to Juno typically transiting northern flux tubes at larger speeds than the southern hemisphere, each northern 1-s measurement corresponds to a greater distance/angular separation, making the spatial resolution lower. As a consequence, the 33% full PA coverage periods do not always coincide with Juno transiting the tail flux tubes, particularly in the north. An example of this is shown in Figure 3 (N5, where N5 corresponds to the top left panel for the northern PJ5 pass). Here while JADE fortuitously maintained complete downward electron PA coverage allowing for continuous downward flux determination, the entirety of the IFPT event coincided with a period when JADE could not measure the upward electron fluxes.

Comparing across the three perijoves, there is a clear difference between the northern and southern passes. Namely, each southern pass exhibits a bifurcation in the electron flux signatures, where an appreciable dip is present during at all PJs. The northern passes do not exhibit this same structure. The difference is most notable in PJ7, but also present in PJ5 and PJ6, particularly once the upward and downward fluxes are separated as discussed below. Due to the higher transit speeds in the north, the JADE-E PA coverage is coarser; therefore, the electron measurements do not preclude the possibility for northern bifurcations. However, as discussed in later in the text, comparisons between the Waves and JADE data suggest that there is stronger evidence

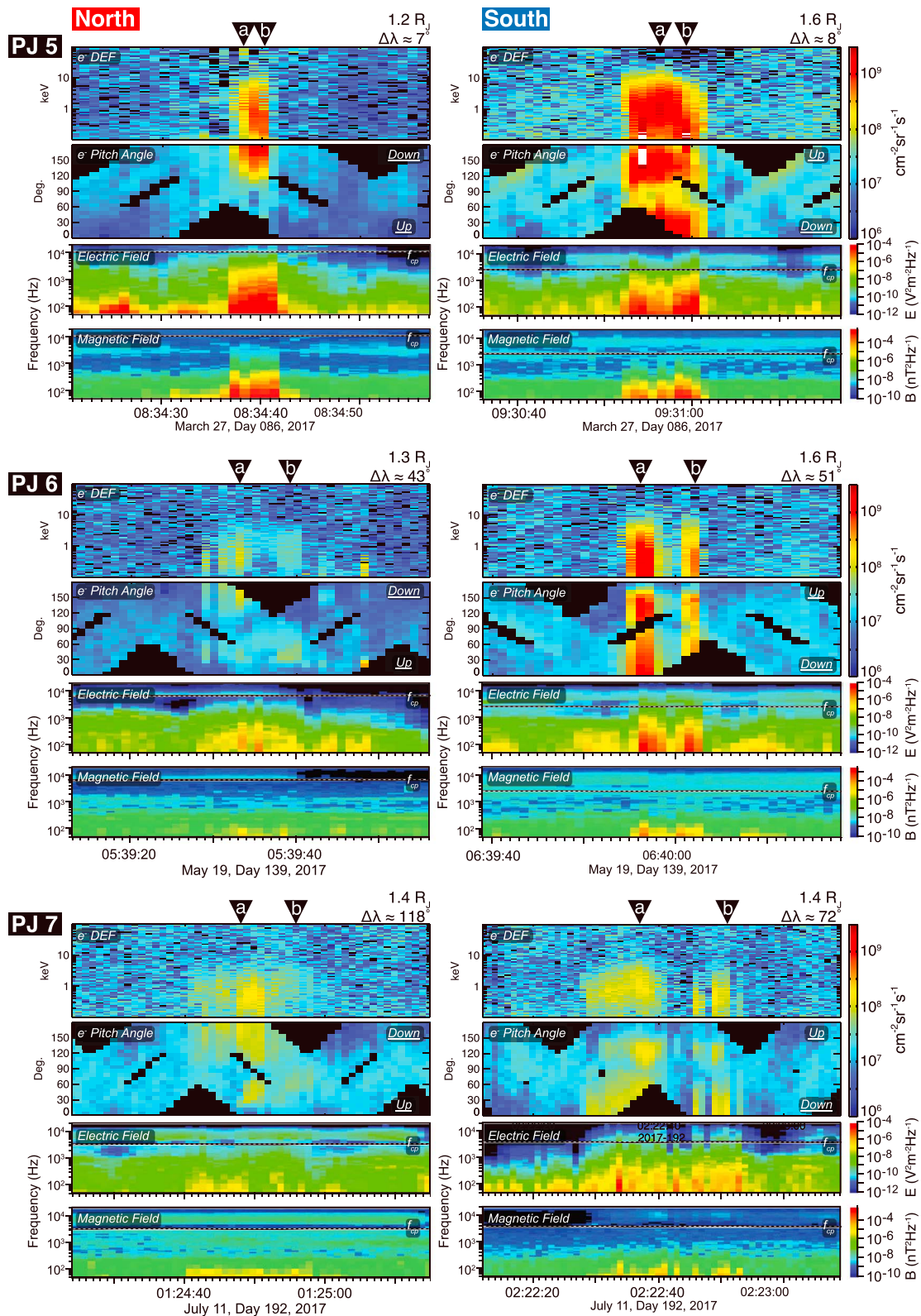


Figure 3. Jovian Auroral Distributions Experiment differential electron energy flux (DEF), electron pitch angle (PA), and electric and magnetic spectrograms covering the frequency range of 50 Hz to 20 kHz for the (left column) northern and (right column) southern passes. The rows correspond to PJ5, PJ6, and PJ7. Text labels at the top right of each panel show Juno's planetocentric distance and separation from the main Alfvén wing. Markers *a* and *b* on each panel denote the times for spectra shown in Figure 5. PJ = perijove.

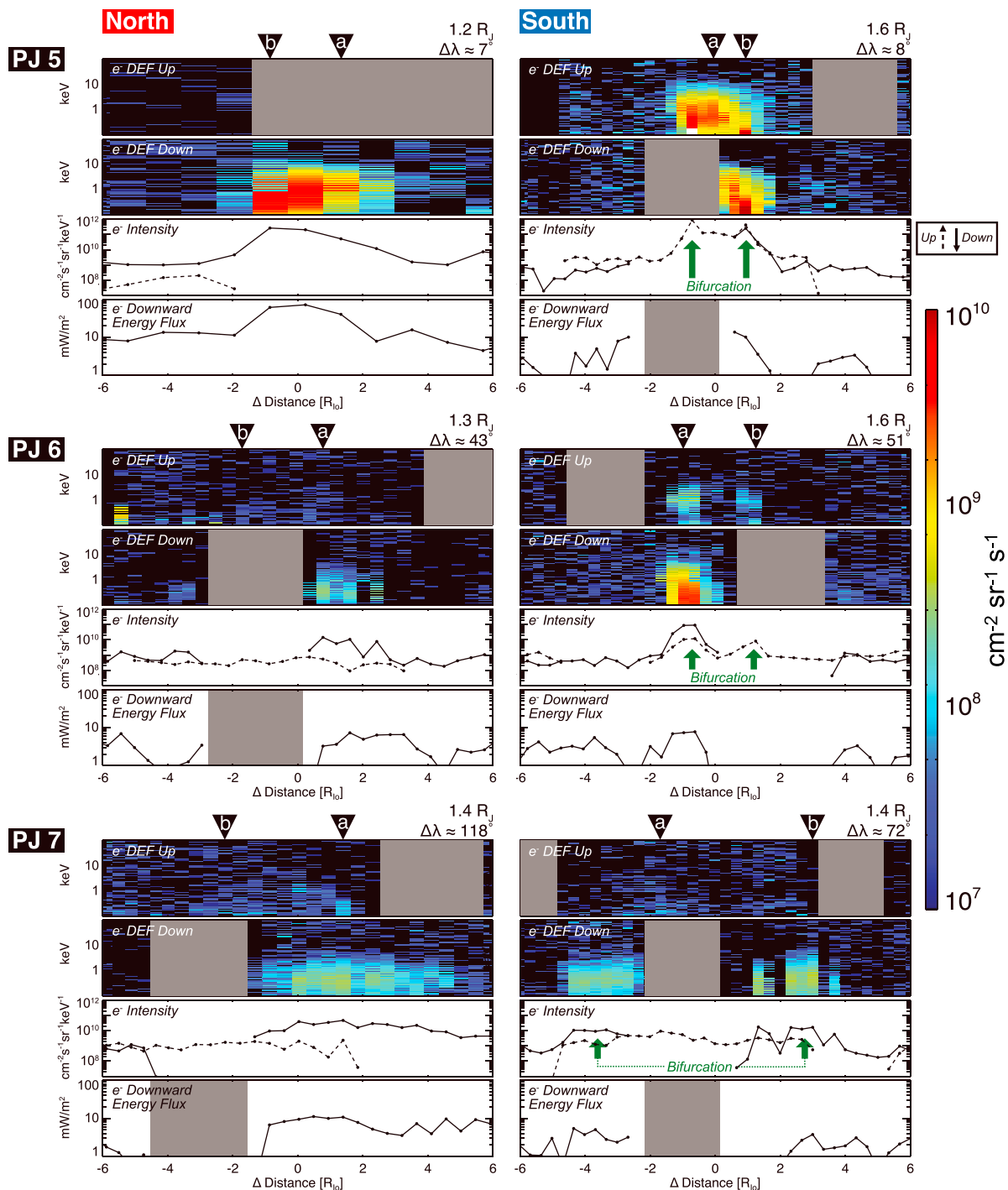


Figure 4. From top to bottom in each of the six panels, electron upward and downward differential energy fluxes, intensities, and downward energy flux as a function of differential M shell from the approximate center of each feature in R_{10} derived from Jovian Auroral Distributions Experiment-E data. Configuration of the panels is the same as Figure 3. Green arrows indicate the peaks of the observed bifurcated structures. DEF = differential electron energy flux; PJ = perijove.

for southern bifurcations than northern. Additionally, the observed electron fluxes were highest when near to the MAW, decreasing as a function of $\Delta\lambda_{\text{J10}}$ as Juno transited the IFPT flux tubes further down the tail.

Figure 4 shows separate upward and downward differential electron energy flux spectrograms in the first and second panels, determined by averaging the three highest and lowest PA bins

corresponding to 0–22.5° and 157.5–180°. The third row in each panel shows the upward and downward intensities, and the fourth row shows the downward total energy flux. Both the intensities and downward energy fluxes are calculated summing over the JADE-E instrument range of 0.1–100 keV. The downward energy flux (F_E) is estimated using previously established techniques described in Mauk et al. (2017) and utilized in Ebert et al. (2017b) to calculate field-aligned fluxes in the polar region. This flux is calculated via $F_E = \pi \sum_i (DEF_i \cdot \Delta E_i)$, where π is the area-projection weighted size of the loss cone above Jupiter's atmosphere, i is the JADE-E energy step, DEF_i is the electron differential energy flux in units of particles $\text{cm}^{-2} \text{s}^{-1} \text{sr}^{-1} \text{keV keV}^{-1}$, and ΔE_i is the width of each individual JADE-E energy passband (or energy bin). These quantities are plotted as a function of VIP4 M shell in units of 10 radii, with the zero location chosen to be the approximate center of each feature, indicated by the Δ distance on the x axis. Jupiter is to the left in all figures. Due to the inherent errors in modeling field lines to determine precisely where Juno is magnetically connected to in the magnetosphere, we only show the relative M shells and do not attempt to align the measurements with an inferred magnetospheric location of the 10 tail.

The duration of each feature is determined visually, chosen when a discernible electron flux is evident in the time-energy spectrograms. Table 1 gives the geometric information for each 10 tail feature, including the start and stop times, radial distances, VIP4 and System III latitudes, and local time of the Juno spacecraft. The sizes of these features are calculated in multiple ways corresponding to Jupiter-based, Juno-based, and magnetospheric-based metrics. Listed in Table 1: $\Delta\theta_{\text{Jup}}$ and w_{Jup} are the latitudinal width in degrees and kilometers, respectively, mapped onto Jupiter using VIP4 magnetic mapping; the two θ_{10} rows list 10 's latitude in VIP4 dipole magnetic and centrifugal coordinates; w_{sc} is the distance Juno traveled during the feature ($v_{\text{sc}}\Delta t$, where v_{sc} is the spacecraft speed and Δt is the feature duration); and ΔM is the difference in M shell from beginning to end of each feature. Error bars for the widths, both mapped to Jupiter (w_{Jup}) and local to the spacecraft (w_{sc}), are calculated as the values within a ± 1 -s time range (the instrument measurement cadence) for the listed boundaries.

Due to Juno's orbital geometry, all 10 tail flux tube measurements were made near dusk (Table 1). The PJ5 measurements were taken closest to the actual 10 flux tube of the three PJs in this study, with predicted angular separations of 7° (N5) and 8° (S5). During N5, JADE measured the largest 10 tail correlated downward energy fluxes of 72 mW/m². This measurement was also the nearest to Jupiter of all 10 tail observations (1.20 R_J) and had the largest relative velocity; therefore, the spatial and temporal resolution is lowest for N5. While JADE was unable to measure any appreciable upward electron fluxes as previously described, the PA spectrogram in Figure 3-N5 does show an asymmetry between PA near 60° (up) and 120° (down), suggesting that the downward flux may have dominated throughout N5.

In the south, due in part to the higher temporal resolution, the S5 data exhibited more substructure than N5. Here JADE was able to measure the downward flux for ~50% of the feature and the entirety of the upward flux. The upward DEF spectrogram and intensity time series (Figure 4-S5) exhibited a double peak in flux, as highlighted with the green arrows, with the peaks attaining about an order of magnitude larger upward number flux than their neighboring points. JADE-E was unable to make measurements of the downward flux through the entirety of the double-peaked structure observed in the upward flux enhancement period. During the period JADE could measure both upward and downward fluxes, the downward electron fluxes peaked at exactly the same location and at nearly the same magnitude as the upward fluxes. The near equivalence of the downward and upward fluxes during the second upward peak suggests that Juno could be within a broadband acceleration region, where comparable upward and downward electron fluxes could be expected for such an acceleration mechanism. The first peak in upward flux could be indicative of a downward flux peak; however, JADE-E was unable to observe this. The Waves measurements, as discussed later, also mimic the bifurcation observed in the upward electron fluxes. While S5 is predicted to be at a nearly identical $\Delta\lambda_{10}$ as N5, the observed peak downward energy flux is ~5 times less at 14 mW/m². 10 's position in the torus is also very similar between the N5 and S5 observations, with centrifugal latitude ~6°. The discrepancy in the magnitude of observed flux may be due to the difference in observing altitude between N5 and S5, where the S5 observations are taken ~0.45 R_J higher than N5. Throughout the S5 measurements, there is evidence for a small upward going loss cone in the range of 7.5° to 22.5°; however, this loss cone is

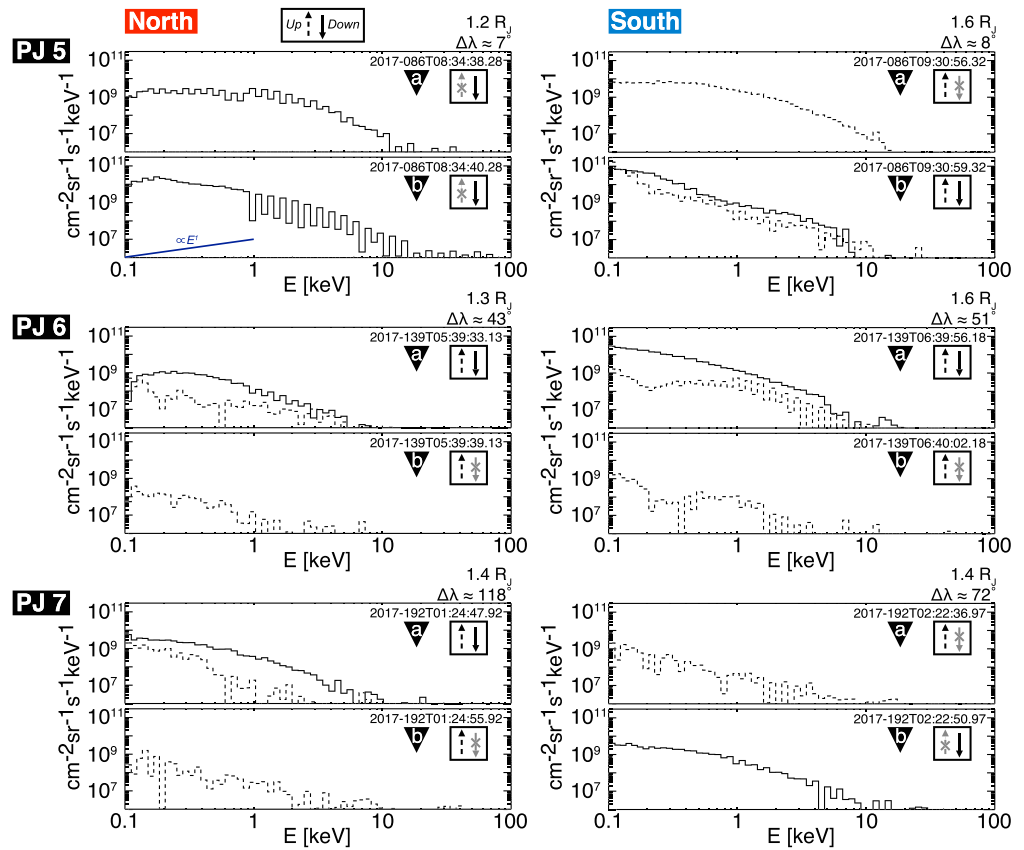


Figure 5. Jovian Auroral Distributions Experiment electron differential intensities ($\text{cm}^{-2} \text{s}^{-1} \text{sr}^{-1} \text{keV}^{-1}$) for two 1-s measurements per hemisphere per PJ, arranged in the same configuration as Figures 2 and 3. The legends in each subpanel show the center timestamp for each measurement, the corresponding letter marker on Figures 2 and 3, and indicate if Jovian Auroral Distributions Experiment was able to observe upward and/or downward going electrons. All downward electron fluxes exhibit broad, power law-like distributions, and nearly always exceed their corresponding upward fluxes. PJ = perijove.

only depleted by a factor of 2–7 from the downward flux for the periods with full PA coverage, exhibiting both upward and downward fluxes.

The measurements during PJ6 and PJ7 were all taken at $\Delta\lambda_{\text{io}} > 40^\circ$. Both of these passes exhibited lower total downward energy fluxes $\sim 10 \text{ mW/m}^2$ and showed similar features such as separate double peaks in each of the southern hemisphere observations, for both upward and downward fluxes when available. While the northern PJ6 total energy flux exhibits a dip in Figure 3-N6 (between the *a* and *b* markers), there is no observable double-peaked structure in the upward and downward fluxes (within 22.5° PA upward/downward) in Figure 4-N6. Given that JADE-E was unable to fully observe the downward energy fluxes during this pass, it is possible PJ6 did have a bifurcated electron feature. However, the lack of clear bifurcation in the Waves data does not suggest a clear bifurcation.

Figure 5 shows specific differential intensity spectra for two 1-s measurement periods per hemisphere per PJ. With the exception of S5b (event b during PJ5 in the south), downward fluxes exceeded upward fluxes by 1 to 2 orders of magnitude, when both were available. The alternating pattern seen in energy spectrograms and spectra (e.g., Figure 5-N5b) is due to electron intensities varying on a faster time scale than the 1-s duty cycle of the instrument. The energies are scanned in a pyramid-like pattern with even steps measured during the up-ramp and the odd steps measured during the down-ramp. Thus, there can be as much as 0.5 s between measurements at adjacent energy steps. This pattern has been observed at multiple locations in the auroral regions where intensities change over a time scale of less than 1-s (e.g., Allegrini et al., 2017) and indicates that fine structure exists in the IFPT on spatial scales less than 20 km.

3.2. Waves Measurements

In addition to the JADE particle instrument, Juno's Waves instrument provides valuable context by characterizing the wave modes encountered during the IFPT auroral transits. Waves utilizes a single electric dipole antenna to detect the electric component of waves in the frequency range of 50 Hz to 41 MHz and a single magnetic search coil to detect the magnetic component of waves in the range of 50 Hz to 20 kHz. The electric antenna's sensitive axis is parallel to the spacecraft **y** axis, while the magnetic search coil's sensitive axis is parallel to the spin axis (spacecraft **z** axis). Survey observations typically provide both an electric and a magnetic spectrum every second in perijove mode, while burst modes can acquire waveforms in various frequency ranges in selected time intervals. Some burst data are selected based on broadband field strength by an onboard algorithm. Typically, burst data are acquired for the magnetic field up to 20 kHz and electric field up to 150 kHz with an additional capability to acquire a 1-MHz band that includes the electron cyclotron frequency. The Waves instrument is further described in Kurth, Hospodarsky, et al. (2017).

The Waves observations for PJ5–PJ7 are shown alongside the JADE-E data in Figure 3. In each panel, frequency is shown on the vertical axis and time on the horizontal axis. The temporal resolution is one spectrum per second for each panel. For each transit, both an electric and a magnetic spectrogram is provided covering the frequency range from 50 Hz to 20 kHz. The color bars for the spectrograms are the same for all of the electric and magnetic panels, respectively. The black and white horizontal line in each Waves spectrogram shows the proton cyclotron frequency. It follows that all of these features are well below the electron cyclotron frequency. Based on indirect evidence, these waves are also below the electron plasma frequency (Kurth, Imai, et al., 2017; Tetrack et al., 2017). Comparing the JADE electron data to the Waves data, it is evident that there is enhanced broadband electromagnetic emission at virtually the same times as the enhanced electron fluxes. The relative intensity of the wave signature shows that temporal variations are highly correlated with the electron fluxes. Even the double-peaked structure clearly evident in the electron fluxes in the southern hemisphere, particularly during PJ6, is reflected in the wave intensities. Similar to the JADE observations, the strongest signature of the Io interaction in the Waves data is found in both hemispheres of PJ5 and the southern hemisphere of PJ6.

3.3. Magnetometer Measurements

Complementing the Waves measurements, Juno's magnetometer (Connerney et al., 2017) allows us to constrain the extent of Alfvénic perturbations in the magnetic field during these periods. Juno transits the Io *M* shells at high latitudes, in the high magnetic field environment near the surface, during which time the instrument operates in its upper dynamic ranges. The minimum magnetic perturbation that can be measured is limited by 16-bit quantization in these ranges (12.5–50 nT in dynamic ranges 4 and 16 G, respectively). With the analysis tools available at present, only spin-averaged quantities are possible. Table 1 lists the spin-averaged magnetic field magnitude $\langle |B| \rangle$ and maximum perpendicular perturbation $|\delta B_{\perp \max}|$ from the magnetometer given the instrument settings for each time. For each of the Io tail events, the magnetometer did not observe any appreciable spin-averaged perpendicular perturbations. Hence, these values give reasonable upper bounds on the extent of Alfvénic perturbations in these regions.

3.4. UVS Observations of Auroral Emissions

We now turn to the remote observations taken by the UVS instrument, which has observed the IFPT during Juno's many flybys (e.g., Bonfond, Gladstone, et al., 2017). While the IFPT aurora (and all aurorae) is typically displayed using 2-D projections mapped onto the polar region, these are three-dimensional phenomena, with each aurora having a radial extent. The vertical dimension of the aurora encodes valuable information about the incident plasma population, as the precipitating populations will preferentially interact with the Jovian atmosphere at varying altitudes depending on their energy distribution. The vertical profile of the Io footprint tail had previously been determined from HST images. On images where the tail is seen above the planetary limb, the brightness peak was found to be 900 km high and the profile could be fitted with a Chapman profile with a large-scale height of 430 km, indicative of a broad precipitating electron energy spectrum (Bonfond et al., 2009).

In the UVS data, the IFPT is rarely seen above the limb and its emissions are usually projected on a polar map for easier visualization of the auroral morphology (e.g., Figure 2). The projection procedure assumes that the auroral emissions are taking place on a thin ellipsoid shell located at a defined altitude above the 1-bar level

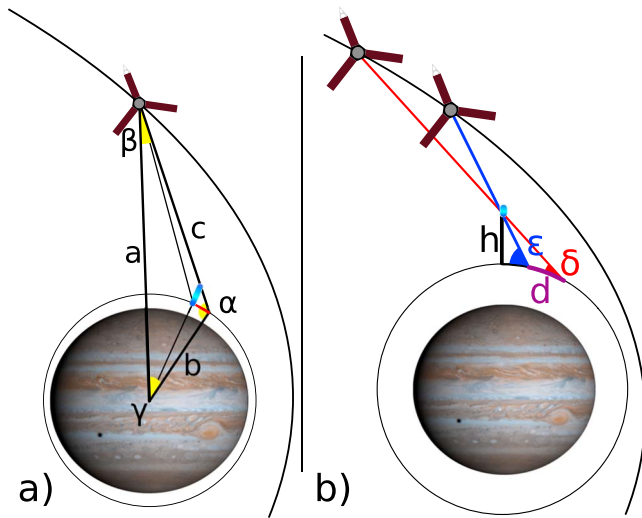


Figure 6. (a) Schematic of the observing geometry in the plane passing through Juno and Jupiter's center and perpendicular to the Io footprint tail. The thin circle outside Jupiter represents the projection ellipsoid. The angle α is deduced from the location of Juno and of the selected auroral feature (i.e., a , b , and γ). (b) Schematic of the geometry used to deduce the altitude of the brightness peak h from the distance d between the projections of this peak on the projection ellipsoid.

(typically 400 km in our case), while they actually have some vertical extent (Figure 6a). Therefore, for auroral features observed from the side, their brightness will be spread out. Since the Juno orbital plane is approximately perpendicular to the Io footprint contour, the spread is essentially in the latitudinal direction. Moreover, if the chosen projection altitude is not appropriate for the auroral feature under consideration, its apparent location will also change as the observation angle evolves (Figure 6b).

An example of this projection effect can be seen on Figure 7 where the middle and right panels show the polar projection at an altitude of 400 km of the Juno-UVS data during one Juno spin from PJ5 on 2017-086 around 08:16 and 08:32:19, respectively. For the middle panel, we combined four consecutive spins in order to increase the signal-to-noise ratio. This can be done because the relative motion of Juno compared to the aurora remains limited at that time. The Juno zenith angle as seen from the IFP tail only varies from 63.6° at 08:15:47 to 62.1° at 08:17:17. The left panel shows a schematic of the observing geometries from these two observations. It can clearly be seen that the apparent location of the IFPT moves poleward, indicating that the emission takes place at a higher altitude than 400 km. The shift h between the actual altitude of the brightness peak and the projection altitude can be deduced from this apparent and (mostly) latitudinal shift d between the peaks from two separate times: $h = \frac{d \tan \delta \tan \epsilon}{\tan \epsilon - \tan \delta}$ (Figure 6), where δ and ϵ are the Juno altitude angle at two different times. In our case, a shift of $d = 1,341$ km corresponds to an altitude of the brightness peak located 460 ± 80 km above the projection altitude (400 km). The observed peak altitude is thus $\sim 860 \pm 80$ km above the 1-

bar level, which is consistent with previous measurements from HST. Such a high peak altitude implies that the precipitating electron mean energy is low (a few kiloelectron volts).

The color ratio between wavelength ranges absorbed (125–130 nm) and unabsorbed (155–162 nm) by methane can also be used to retrieve useful information on the depth from which the emission originates. The higher the energy of electrons is, the deeper they deposit their energy in the atmosphere. The resulting UV emission is more absorbed by the methane present in the lowest parts of the atmosphere. A comparison

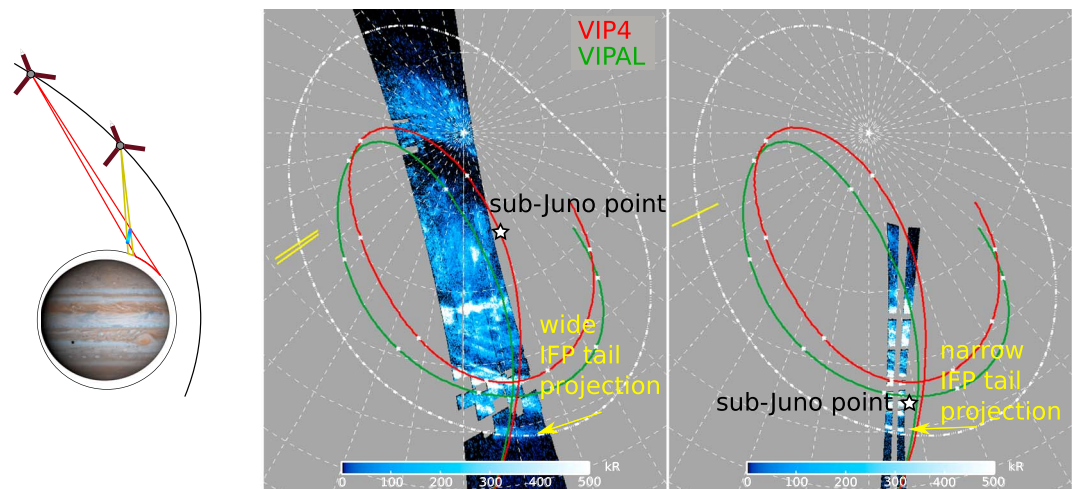


Figure 7. (left panel) Schematic of the observing geometry for the two observations displayed on the middle and right panels. As Juno approaches the auroral feature, the projection onto a reference ellipsoid located at a lower altitude gets narrower and moves toward the pole. (middle) The combination of four individual Juno spins during PJ5 at 2017-086 from 08:15:47 to 08:17:17. (right) A single spin acquired at 08:32:19. The projection altitude is 400 km. The Io footprint reference contour facilitates the visualization of the apparent poleward motion of the Io footprint tail.

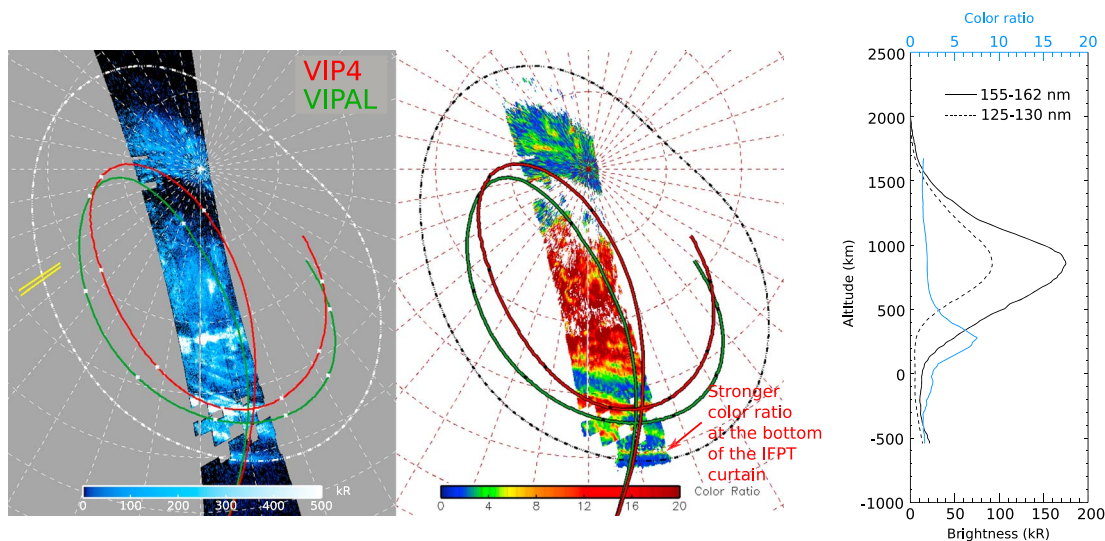


Figure 8. Polar projections of the (left) brightness and (middle) color ratio maps for Ultraviolet Spectrograph observations carried out between 08:15 and 08:17 during the PJ5 northern pass. These maps are based on the sum of four consecutive Juno spins (see Figure 7, middle panel). While the brightness peak is located on the Io footprint reference contour, the corresponding color ratio remains small for the Io footprint tail, except for its apparent polarmost edge, which corresponds to the lower altitudes of the auroral curtain. The right plot shows the mean brightness profiles for two wavelength ranges as well as the color ratio on a scale where the apparent horizontal extent of the emission is converted into altitude. Contrary to the 155- to 162-nm brightness, the 125- to 130-nm brightness rapidly falls below 300 km due to methane absorption.

between the brightness peak in the unabsorbed range and the color ratio peak shows a clear shift, indicating that the bottom of the auroral curtain reaches the methane-rich layers while most of the emission lies well above them (Figure 8). The absorption signatures at the lowest altitudes of the IFPT imply that part of the precipitating electrons have energies on the order of several tens to hundreds of kiloelectron volts (e.g., Gérard et al., 2014). Overall, the UVS measurements corroborate previous HST measurements, providing confirmation that the IFPT-producing electron distribution is broad in energy.

4. Discussion and Conclusions

One of the most striking features in the Juno IFPT data is the observation of broad, power law-like electron distributions and lack of evidence for a broad parallel acceleration process driving the Io tail aurora. This key result favors a more broadband acceleration mechanism, such as Alfvénic acceleration (e.g., Bonfond et al., 2009; Bonfond, Saur, et al., 2017; Cray & Bagenal, 1997; Jacobsen et al., 2007, 2010), instead of large-scale parallel potential structures accelerating electrons near the IFPT. As shown in Figure 5, the downward electron fluxes have a strong power law-like character and do not exhibit the canonical inverted-V signatures or peaked potentials in the 1- to 100-keV range. This finding suggests that the acceleration process driving the Io footprint tail aurora is characteristically more broadband, possibly driven by an Alfvénic acceleration process (Bonfond, Saur, et al., 2017). Such processes lead to power law distributions that extend to high (hundreds of kiloelectron volts) energies through turbulent cascading processes (Hess et al., 2010; Saur et al., 2002). This is similar to the broadband acceleration processes of Jupiter's main auroral oval (Mauk et al., 2017; Mauk & Saur, 2007; Saur et al., 2003). By combining measurements of the tail's vertical profile above the planetary limb with Monte Carlo simulations of the emission profile, Bonfond et al. (2009) and Bonfond, Saur, et al. (2017) concluded that the incident electron energy distribution is broad and consistent with a kappa distribution rather than a narrower Maxwellian distribution. The Juno/UVS measurements discussed in this study further corroborate the previous HST estimates of the vertical extent of the emissions. In general, these observations seem to fit the recently emerging understanding of Jovian auroral processes, which have been observed to have occasional parallel potential structures, analogous to Earth's aurora, yet are dominated by more broadband acceleration mechanisms (Mauk et al., 2017).

While JADE did not observe a large-scale inverted-V spanning across the entire IFPT, these measurements cannot directly address whether or not small-scale inverted-V structures exist below the spacecraft

resolution. With 1-s resolution and Juno traveling approximately 50 km/s during these times, JADE samples local structures ~50 km local to the spacecraft. At Earth, the FAST spacecraft was able to sample auroral structures ~1 km local to the spacecraft. When transiting regions with large Alfvénic acceleration structures, FAST observed small-scale, localized parallel electric fields (Ergun et al., 2005). It is likely that more complex substructure exists below the JADE resolution, possibly analogous to the phenomena observed by FAST at Earth. While resolving such fine substructure is beyond the nominal measurement capabilities of the Juno instrument suite, the *checkerboard* pattern observed in the electron data provides at least indirect evidence of substructure below 20 km.

The JADE electron observations rule out a large-scale, quasi-static, parallel acceleration process spanning the cross section of the IFPT. Observations of a power law-like distribution strongly indicate but do not unambiguously determine if the local acceleration process is Alfvénic. The magnetic field measurements with upper limits of 6–25 nT are preliminarily consistent with values of 10 nT in the model of the main footprint by Hess et al. (2010). If we assume a decay along the tail with an angular scale length of 12° (e.g., Bonfond, Saur, et al., 2017), the model value reduces to ~6 nT at a crossing of the tail 7° downstream of the main spot.

Additionally, the JADE data can be utilized to infer the location of the acceleration region causing the IFPT aurora by comparing the measurements taken near the MAW ($\sim 10^\circ$, N5, and S5) and those taken farther down tail (40° to 120° , N6–7, and S6–7). As shown in Figure 5–S5b, JADE observed nearly equal upward and downward electron fluxes during S5, both with strong power law character and approximate differential intensity slopes of -2.0 . This slope is reasonably consistent with the estimates of Bonfond et al. (2009), which predicted a slope of -2.3 based on the auroral vertical brightness profile. The existence of a strong upward electron flux and symmetry of the structure and slope with the downward flux suggests that comparable quantities of electrons are being accelerated both above and below Juno at $1.4 R_J$ (distance measured from the center of the planet) via similar mechanisms. This points to a broadband acceleration region that may extend both above and below $1.4 R_J$ near the MAW.

For measurements obtained further down tail, JADE consistently measured depleted loss cones of $20\text{--}30^\circ$ with 10–100 times larger downward electron fluxes than upward and power law-like downward electron distributions. These measurements, made at $\Delta\lambda_{\text{Io}} > 40^\circ$ down tail, suggest that the majority of the acceleration is also of broadband origin and has occurred above the Juno spacecraft's planetocentric radial distance of $1.26\text{--}1.65 R_J$. This is consistent with theoretical predictions that the peak in parallel Alfvénic acceleration would occur at $1.5\text{--}1.9 R_J$, with a large portion of the acceleration occurring above this distance (Hess et al., 2010; Jones & Su, 2008).

With respect to the Waves data, we note that given the large background wave spectrum, perhaps due to whistler mode hiss, it is difficult to clearly identify the specific wave modes in the Waves data during the IFPT transits. These measurements are not entirely suitable to fully characterize the wave character given the observation geometry and current state of analysis tools. Additionally, much of the relevant waves activity may occur at frequencies lower than the Waves instruments limit of 50 Hz. Reconciling these observations with the particle data will be important to ongoing interpretations of the IFPT.

With respect to the observed energy fluxes, modeling HST emissions have produced a rule-of-thumb guide that an electron energy flux of 1 mW/m^2 injected at the top of Jupiter's atmosphere should produce an H_2 UV auroral brightness of roughly 10 kR (Grodent et al., 2001; Gustin et al., 2012). For the MAW spot, Bonfond et al. (2013) measured a maximum brightness in excess of several MR and derived typical incoming electron energy fluxes between 250 and $2,000 \text{ mW/m}^2$. For the IFPT, Bonfond et al. (2009) estimated injected energy fluxes between 2 and 20 mW/m^2 . The fluxes measured by JADE of 7 to 72 mW/m^2 are therefore in full agreement with the typical UV auroral brightness of the different components of Io's auroral footprint. Specifically, the larger JADE flux value, 72 mW/m^2 , was obtained when Juno was on field lines mapping to a region very close to, but not directly on the MAW, where the brightness is still high compared to the tail emission.

Turning to the geometry of the IFPT, the JADE and Waves measurements can also be used as an independent measure of the tail width as a function of longitudinal separation down tail. Mapping the spacecraft location at the boundaries outlined in Table 1 back to Jupiter, the widths of the electron features measured by JADE-E can be converted to latitudinal widths. These widths are also consistent with the Waves electric field

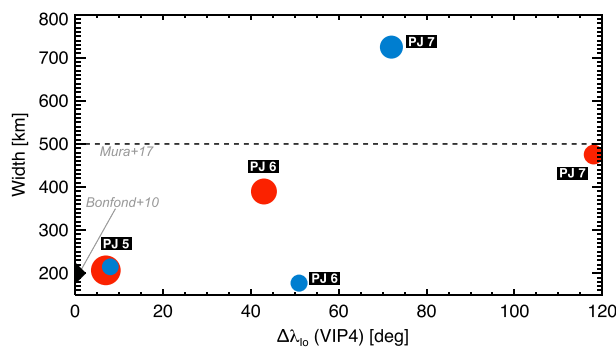


Figure 9. Widths of the Jovian Auroral Distributions Experiment features mapped to Jupiter as a function of tail longitudinal separation for the northern (red) and southern (blue) passes during PJ5–PJ7. Also shown is the constant thickness of 500 km observed by Jovian Infrared Auroral Mapper (Mura et al., 2017) during Juno’s PJ1 pass and the Hubble Space Telescope observed main Alfvén wing thickness of 200 km (Bonfond, 2010). The size of each circle corresponds to its error in width. PJ = perijove.

perturbation structures. Figure 9 shows these widths as a function of $\Delta\lambda_{Io}$ along with the constant value of 500 km observed by the Jovian Infrared Auroral Mapper aboard Juno (Mura et al., 2017). The electron and wave structures Juno transited exhibited a general trend of increasing width with longitudinal separation, consistent at small $\Delta\lambda_{Io}$ with previous HST measurements of the MAW spot thickness of ~ 200 km (Bonfond, 2010) and increasing to ~ 500 – 700 km for $\Delta\lambda_{Io}$ in the range of 70° to 120° . This broadening could be caused by multiple reflections of the Alfvén waves with subsequent scattering and drifts of the accelerated electrons. It could also be a consequence of Alfvénic filamentation (Chust et al., 2005), which could serve to disperse the tail features as they evolve down the tail.

Finally, we turn to the bifurcated tail structure observed in all southern passes. While the low-energy electron PA coverage is modulated by the Juno spin phase, a persistent double-peaked structure exists in JADE data for all southern passes that is not tied to this modulation. These features are also observed in the electric field perturbations measured by the Waves instrument. While there is no clear bifurcation in the upward/downward fluxes during the northern PJ6 pass, there is a dip in

the observed electron DEF spectrogram that could potentially suggest a bifurcation in the north for this period. This feature could be due to a sampling artifact due to the incomplete PA coverage or could suggest a real bifurcation exists. However, the Waves data do not indicate a clear bifurcation for this period. The fine structure observed primarily in the south may be a direct consequence of the Alfvén wave intensity having a maximum on both flanks of Io (e.g., Saur et al., 2013; Jacobsen et al., 2007), leading naturally to a double-peaked intensity profile as Alfvén waves generated from different locations would experience slightly different conditions throughout the multiple reflection geometry. However, this double-peaked feature may also be a direct by-product of the subcorotational flow downstream of Io (Delamere et al., 2003; Ergun et al., 2009). If sufficient shears exist between subcorotational flow directly along the Io wake and adjacent radial distances which are fully corotational, shear-related eddies may form that may be sufficiently small in scale to produce large Alfvénic disturbances. The latitudinal scale of these substructures is on the order of 100 km when mapped to Jupiter, which is smaller than the point-spread function of the UVS instrument. Resolving such substructure, therefore, is very challenging with the UV data. The lack of clear bifurcation signatures in the northern hemisphere during PJ5–PJ7 could indicate that this bifurcation manifests transiently or its manifestation is obscured by the northern magnetic anomaly (Grodent et al., 2008). We note that recent Jovian Infrared Auroral Mapper observations found evidence of a split tail in the north, yet not in the south (Mura et al., 2018) for a different subset of Juno flybys than studied in this work. Future comparisons between coincident measurements with both the in situ and remote sensing instruments aboard Juno will be critical to understanding the nature of the tail.

The Juno measurements through the Io tail revealed rich substructure and point to a broadband mechanism for the electrons producing the Io tail aurora, while additional mysteries still exist on the precise nature of this acceleration. Our results are summarized in the following key points:

1. The electrons responsible for generating the IFPT aurora have a broad energy distribution, consistent with a dominantly broadband, possibly Alfvénic, acceleration mechanism;
2. No large-scale, parallel potential structures are observed connected to the IFPT;
3. The electron energy fluxes inferred with JADE measurements are consistent with the observed values derived from IFPT auroral brightness observations;
4. Near the MAW at $\Delta\lambda_{Io} \approx 10^\circ$, the acceleration region extends below $1.4 R_J$, while farther down the tail at $\Delta\lambda_{Io} > 40^\circ$, the acceleration region must exist above planetocentric distances of 1.26 – $1.65 R_J$;
5. Fine structure is observed on scales of ~ 20 km mapped to the 1-bar level in the cross-tail direction;
6. All southern passes observed in this work exhibited a dual-peaked structure in the electron and waves data, indicating bifurcation of the tail;
7. The northern PJ6 pass exhibits a weak dip in the differential energy flux, potentially indicating a minor northern bifurcation during this flyby;
8. The IFPT is observed to widen, from ~ 200 km near the MAW to 500 – 700 km at $\Delta\lambda_{Io} > 70^\circ$.

The lack of evidence for a broad-scale parallel acceleration mechanism fits the newly developing view of Jovian magnetospheric acceleration processes, which in the Juno data so far appear to be dominated by more broadband acceleration (Mauk et al., 2017). Juno measurements through the IFPT, other foot point tails such as Europa's and Ganymede's, and polar auroral structures will further elucidate the underlying physics in these complex phenomena.

Acknowledgments

The authors would like to thank many Juno team members that made these observations possible. We also thank Rahul Kumar for the insightful discussions on wave-particle interactions and Drake Ranquist for the magnetic field mapping codes. The Juno data used in this study can be obtained from the Planetary Data System (PDS) at <http://pds.nasa.gov/>. B. B. and D.G. acknowledge financial support from the Belgian Federal Science Policy Office (BELSPO) via the PRODEX Programme of ESA. B.B. is a Research Associate of the Fonds de la Recherche Scientifique - FNRS. The research efforts at the University of Iowa and University of Colorado are supported by NASA through Contracts 699041X and 699050X with the Southwest Research Institute. We thank two anonymous reviewers for their constructive comments.

References

- Acuna, M. H., Neubauer, F. M., & Ness, N. F. (1981). Standing Alfvén wave current system at Io—Voyager 1 observations. *Journal of Geophysical Research*, 86, 8513–8521. <https://doi.org/10.1029/JA086iA10p08513>
- Allegri, F., Bagenal, F., Bolton, S., Connerney, J., Clark, G., Ebert, R. W., et al. (2017). Electron beams and loss cones in the auroral regions of Jupiter. *Geophysical Research Letters*, 44, 1–9. <https://doi.org/10.1002/2017GL073180>
- Bagenal, F. (1983). Alfvén wave propagation in the Io plasma torus. *Journal of Geophysical Research*, 88, 3013–3025. <https://doi.org/10.1029/JA088iA04p03013>
- Bagenal, F., Adriani, A., Allegri, F., Bolton, S. J., Bonfond, B., Bunce, E. J., et al. (2014). Magnetospheric science objectives of the Juno mission. *Space Science Reviews*, 213(1–4), 219–287. <https://doi.org/10.1007/s11214-014-0036-8>
- Belcher, J. W., Goertz, C. K., Sullivan, J. D., & Acuna, M. H. (1981). Plasma observations of the Alfvén wave generated by Io. *Journal of Geophysical Research*, 86, 8508–8512. <https://doi.org/10.1029/JA086iA10p08508>
- Bigg, E. K. (1964). Influence of the satellite Io on Jupiter's decametric emission. *Nature*, 203(4949), 1008–1010. <https://doi.org/10.1038/2031008a0>
- Bonfond, B. (2010). The 3-D extent of the Io UV footprint on Jupiter. *Journal of Geophysical Research*, 115, A09217. <https://doi.org/10.1029/2010JA015475>
- Bonfond, B., Gladstone, G. R., Grodent, D., Greathouse, T. K., Versteeg, M. H., Hue, V., et al. (2017). Morphology of the UV aurorae Jupiter during Juno's first perijove observations. *Geophysical Research Letters*, 44, 4463–4471. <https://doi.org/10.1002/2017GL073114>
- Bonfond, B., Grodent, D., Gérard, J.-C., Radioti, A., Dols, V., Delamere, P. A., & Clarke, J. T. (2009). The Io UV footprint: Location, inter-spot distances and tail vertical extent. *Journal of Geophysical Research*, 114, A07224. <https://doi.org/10.1029/2009JA014312>
- Bonfond, B., Grodent, D., Gérard, J. C., Radioti, A., Saur, J., & Jacobsen, S. (2008). UV Io footprint leading spot: A key feature for understanding the UV Io footprint multiplicity? *Geophysical Research Letters*, 35, L05107. <https://doi.org/10.1029/2007GL032418>
- Bonfond, B., Hess, S., Gérard, J. C., Grodent, D., Radioti, A., Chantry, V., et al. (2013). Evolution of the Io footprint brightness I: Far-UV observations. *Planetary and Space Science*, 88, 64–75. <https://doi.org/10.1016/j.pss.2013.05.023>
- Bonfond, B., Saur, J., Grodent, D., Badman, S. V., Bisikalo, D., Shmatovich, V., et al. (2017). The tails of the satellite auroral footprints at Jupiter. *Journal of Geophysical Research: Space Physics*, 122, 7985–7996. <https://doi.org/10.1002/2017JA024370>
- Chust, T., Roux, A., Kurth, W. S., Gurnett, D. A., Kivelson, M. G., & Khurana, K. K. (2005). Are Io's Alfvén wings filamented? Galileo observations. *Planetary and Space Science*, 53(4), 395–412. <https://doi.org/10.1016/j.pss.2004.09.021>
- Clarke, J. T., Ballester, G. E., Trauger, J., Evans, R., Connerney, J. E. P., Stapelfeldt, K., et al. (1996). Far-ultraviolet imaging of Jupiter's aurora and the Io "footprint". *Science*, 274(5286), 404–409. <https://doi.org/10.1126/science.274.5286.404>
- Connerney, J. E. P., Acuna, M. H., & Ness, N. F. (1981). Modeling the Jovian current sheet and inner magnetosphere. *Journal of Geophysical Research*, 86, 8370–8384. <https://doi.org/10.1029/JA086iA10p08370>
- Connerney, J. E. P., Acuna, M. H., Ness, N. F., & Satoh, T. (1998). New models of Jupiter's magnetic field constrained by the Io flux tube footprint. *Journal of Geophysical Research*, 103, 11,929–11,939. <https://doi.org/10.1029/97JA03726>
- Connerney, J. E. P., Baron, R., Satoh, T., & Owen, T. (1993). Images of excited H₃⁺ at the foot of the Io flux tube in Jupiter's atmosphere. *Science*, 262(5136), 1035–1038. <https://doi.org/10.1126/science.262.5136.1035>
- Connerney, J. E. P., Benn, M., Bjarno, J. B., Denver, T., Espley, J., Jorgensen, J. L., et al. (2017). The Juno magnetic field investigation. *Space Science Reviews*, 213(1–4), 39–138. <https://doi.org/10.1007/s11214-017-0334-z>
- Connerney, J. E. P., & Satoh, T. (2000). The H₃⁺ ion: A remote diagnostic of the Jovian magnetosphere. *Philosophical Transactions of the Royal Society London A*, 358(1774), 2471–2483. <https://doi.org/10.1098/rsta.2000.0661>
- Crary, F. J. (1997). On the generation of an electron beam by Io. *Journal of Geophysical Research*, 102, 37–49. <https://doi.org/10.1029/96JA02409>
- Crary, F. J., & Bagenal, F. (1997). Coupling the plasma interaction at Io to Jupiter. *Geophysical Research Letters*, 24, 2135–2138. <https://doi.org/10.1029/97GL02248>
- Das, A. C., & Ip, W. H. (1992). Particle acceleration by kinetic Alfvén waves in the Io plasma torus. *Planetary and Space Science*, 40(11), 1499–1502. [https://doi.org/10.1016/0032-0633\(92\)90046-Q](https://doi.org/10.1016/0032-0633(92)90046-Q)
- Delamere, P. A., Bagenal, F., Ergun, R. E., & Su, Y. J. (2003). Momentum transfer between the Io plasma wake and Jupiter's ionosphere. *Journal of Geophysical Research*, 108(A6), 1241. <https://doi.org/10.1029/2002JA009530>
- Ebert, R. W., Allegri, F., Bagenal, F., Bolton, S. J., Connerney, J. E. P., Clark, G., et al. (2017a). Accelerated flows at Jupiter's magnetopause: Evidence for magnetic reconnection along the Dawn flank. *Geophysical Research Letters*, 44, 4401–4409. <https://doi.org/10.1002/2016GL072187>
- Ebert, R. W., Allegri, F., Bagenal, F., Bolton, S. J., Connerney, J. E. P., Clark, G., et al. (2017b). Spatial distribution and properties of 0.1–100 keV electrons in Jupiter's polar aurora region. *Geophysical Research Letters*, 44, 9199–9207. <https://doi.org/10.1002/2017GL075106>
- Ergun, R. E., Andersson, L., Su, Y. J., Newman, D. L., Goldman, M. V., Lotko, W., et al. (2005). Localized parallel electric fields associated with inertial Alfvén waves. *Physics of Plasmas*, 12(7), 072,901–072,907. <https://doi.org/10.1063/1.1924495>
- Ergun, R. E., Ray, L., Delamere, P. A., Bagenal, F., Dols, V., & Su, Y. J. (2009). Generation of parallel electric fields in the Jupiter-Io torus wake region. *Journal of Geophysical Research*, 114, A05201. <https://doi.org/10.1029/2008JA013968>
- Frank, L. A., & Paterson, W. R. (1999). Intense electron beams observed at Io with the Galileo spacecraft. *Journal of Geophysical Research*, 104, 28,657–28,669. <https://doi.org/10.1029/1999JA900402>
- Gérard, J.-C., Bonfond, B., Grodent, D., Radioti, A., Clarke, J. T., Gladstone, G. R., et al. (2014). Mapping the electron energy in Jupiter's aurora: Hubble spectral observations. *Journal of Geophysical Research: Space Physics*, 119, 9072–9088. <https://doi.org/10.1002/2014JA020514>
- Gershman, D. J., DiBraccio, G. A., Connerney, J. E. P., Hospodarsky, G., Kurth, W. S., Ebert, R. W., et al. (2017). Juno observations of large-scale compressions of Jupiter's dawnside magnetopause. *Geophysical Research Letters*, 44, 7559–7568. <https://doi.org/10.1002/2017GL073132>
- Gladstone, G. R., Persyn, S. C., Eterno, J. S., Walther, B. C., Slater, D. C., Davis, M. W., et al. (2017). The ultraviolet spectrograph on NASA's Juno mission. *Space Science Reviews*, 213(1–4), 447–473. <https://doi.org/10.1007/s11214-014-0040-z>

- Goldreich, P., & Lynden-Bell, D. (1969). Io, a Jovian unipolar inductor. *Astrophysical Journal*, 156(1P1), 59–78. <https://doi.org/10.1086/149947>
- Grodent, D. (2015). A brief review of ultraviolet auroral emissions on giant planets. *Space Science Reviews*, 187(1), 23–50. <https://doi.org/10.1007/s11214-014-0052-8>
- Grodent, D., Bonfond, B., Gérard, J.-C., Radioti, A., Gustin, J., Clarke, J. T., et al. (2008). Auroral evidence of a localized magnetic anomaly in Jupiter's northern hemisphere. *Journal of Geophysical Research*, 113, A09201. <https://doi.org/10.1029/2008JA013185>
- Grodent, D., Waite, J. H. Jr., & Gérard, J.-C. (2001). A self-consistent model of the Jovian auroral thermal structure. *Journal of Geophysical Research*, 106, 12,933–12,952.
- Gurnett, D. A., & Goertz, C. K. (1981). Multiple Alfvén wave reflections excited by Io origin of the Jovian decametric arcs. *Journal of Geophysical Research*, 86, 717–722. <https://doi.org/10.1029/JA086iA02p00717>
- Gustin, J., Bonfond, B., Grodent, D., & Gérard, J. C. (2012). Conversion from HST ACS and STIS auroral counts into brightness, precipitated power and radiated power for H₂ giant planets. *Journal of Geophysical Research*, 117, A07316. <https://doi.org/10.1029/2012JA017607>
- Hess, S. L. G., Bonfond, B., Zarka, P., & Grodent, D. (2011). Model of the Jovian magnetic field topology constrained by the Io auroral emissions. *Journal of Geophysical Research*, 116, A05217. <https://doi.org/10.1029/2010JA016262>
- Hess, S. L. G., Delamere, P., Dols, V., Bonfond, B., & SwIFT, D. (2010). Power transmission and particle acceleration along the Io flux tube. *Journal of Geophysical Research*, 115, A06205. <https://doi.org/10.1029/2009JA014928>
- Hill, T. W., & Vasyliunas, V. M. (2002). Jovian auroral signature of I_o's corotational wake. *Journal of Geophysical Research*, 107(A12), 1464. <https://doi.org/10.1029/2002JA009514>
- Jacobsen, S., Neubauer, F. M., Saur, J., & Schilling, N. (2007). Io's nonlinear MHD-wave field in the heterogeneous Jovian magnetosphere. *Geophysical Research Letters*, 34, L10202. <https://doi.org/10.1029/2006GL029187>
- Jacobsen, S., Saur, J., Neubauer, F. M., Bonfond, B., Gérard, J.-C., & Grodent, D. (2010). Location and spatial shape of electron beams in Io's wake. *Journal of Geophysical Research*, 115, A04205. <https://doi.org/10.1029/2010JA015475>
- Jones, S. T., & Su, Y.-J. (2008). Role of dispersive Alfvén waves in generating parallel electric fields along the Io-Jupiter flux tube. *Journal of Geophysical Research*, 113, A12205. <https://doi.org/10.1029/2008JA013512>
- Kurth, W. S., Hospodarsky, G. B., Kirchner, D. L., Mokrzycki, B. T., Averkamp, T. F., Robison, W. T., et al. (2017). The Juno Waves investigation. *Space Science Reviews*, 213(1–4), 347–392. <https://doi.org/10.1007/s11214-017-0396-y>
- Kurth, W. S., Imai, M., Hospodarsky, G. B., Gurnett, D. A., Louarn, P., Valek, P., et al. (2017). A new view of Jupiter's auroral radio spectrum. *Geophysical Research Letters*, 44, 7114–7121. <https://doi.org/10.1002/2017GL072889>
- Louarn, P., Allegrini, F., McComas, D. J., Valek, P. W., Kurth, W. S., André, N., et al. (2017). Generation of the Jovian hectometric radiation: First lessons from Juno. *Geophysical Research Letters*, 44, 4439–4446. <https://doi.org/10.1002/2017GL072923>
- Matsuda, K., Terada, N., Kato, Y., & Misawa, H. (2012). A simulation study of the current-voltage relationship of the Io tail aurora. *Journal of Geophysical Research*, 117, A10214. <https://doi.org/10.1029/2012JA017790>
- Mauk, B. H., Haggerty, D. K., Paranicas, C., Clark, G., Kollmann, P., Rymer, A. M., et al. (2017). Discrete and broadband electron acceleration in Jupiter's powerful aurora. *Nature*, 549(7670), 66–69. <https://doi.org/10.1038/nature23648>
- Mauk, B. H., & Saur, J. (2007). Equatorial electron beams and auroral structuring at Jupiter. *Journal of Geophysical Research*, 112, A10221. <https://doi.org/10.1029/2007JA012370>
- Mauk, B. H., Williams, D. J., & Eviatar, A. (2001). Understanding Io's space environment interaction: Recent energetic electron measurements from Galileo. *Journal of Geophysical Research*, 106, 26,195–26,208. <https://doi.org/10.1029/2000JA002508>
- McComas, D. J., Alexander, N., Allegrini, F., Bagenal, F., Beebe, C., Clark, G., et al. (2017). The Jovian Auroral Distributions Experiment (JADE) on the Juno mission to Jupiter. *Space Science Reviews*, 213(1–4), 547–643. <https://doi.org/10.1007/s11214-013-9990-9>
- McComas, D. J., Szalay, J., Allegrini, F., Bagenal, F., Connerney, J. E. P., Ebert, R. W., et al. (2017). Plasma environment at the dawn flank of Jupiter's magnetosphere: Juno arrives at Jupiter. *Geophysical Research Letters*, 44, 4432–4438. <https://doi.org/10.1002/2017GL072831>
- Mura, A., Adriani, A., Altieri, F., Connerney, J. E. P., Bolton, S. J., Moriconi, M. L., et al. (2017). Infrared observations of Jovian aurora from Juno's first orbits: Main oval and satellite footprints. *Geophysical Research Letters*, 44, 5308–5316. <https://doi.org/10.1002/2017GL072954>
- Mura, A., Adriani, A., Connerney, J. E. P., Bolton, S., Altieri, F., Bagenal, F., et al. (2018). Juno observations of spot structures and a split tail in Io-induced aurorae on Jupiter. *Science*, 361(6404), 774–777. <https://doi.org/10.1126/science.aat1450>
- Neubauer, F. M. (1980). Nonlinear standing Alfvén wave current system at Io—Theory. *Journal of Geophysical Research*, 85, 1171–1178. <https://doi.org/10.1029/JA085iA03p01171>
- Neubauer, F. M. (1998). The sub-Alfvénic interaction of the Galilean satellites with the Jovian magnetosphere. *Journal of Geophysical Research*, 103, 19,843–19,866. <https://doi.org/10.1029/97JE03370>
- Saur, J., Grambusch, T., Duling, S., Neubauer, F. M., & Simon, S. (2013). Energy fluxes in sub-Alfvénic planet star and moon planet interactions. *Astronomy and Astrophysics*, 552, A119. <https://doi.org/10.1051/0004-6361/201118179>
- Saur, J., Politano, H., Pouquet, A., & Matthaeus, W. H. (2002). Evidence for weak MHD turbulence in the middle magnetosphere of Jupiter. *Astronomy and Astrophysics*, 386(2), 699–708. <https://doi.org/10.1051/0004-6361:20020305>
- Saur, J., Pouquet, A., & Matthaeus, W. H. (2003). An acceleration mechanism for the generation of the main auroral oval on Jupiter. *Geophysical Research Letters*, 30(5), 1260. <https://doi.org/10.1029/2002GL015761>
- Su, Y.-J., Ergun, R. E., Bagenal, F., & Delamere, P. A. (2003). Io-related Jovian auroral arcs: Modeling parallel electric fields. *Journal of Geophysical Research*, 108(A2), 1094. <https://doi.org/10.1029/2002JA009247>
- Szalay, J. R., Allegrini, F., Bagenal, F., Bolton, S., Clark, G., Connerney, J. E. P., et al. (2017). Plasma measurements in the Jovian polar region with Juno/JADE. *Geophysical Research Letters*, 44, 7122–7130. <https://doi.org/10.1002/2017GL072837>
- Tetrick, S., Gurnett, D. A., Kurth, W. S., Imai, M., Hospodarsky, G. B., Bolton, S. J., et al. (2017). Plasma waves in Jupiter's high latitude regions: Observations from the Juno spacecraft. *Geophysical Research Letters*, 44, 4447–4454. <https://doi.org/10.1002/2017GL073073>
- Valek, P. W., Thomsen, M. F., Allegrini, F., Bagenal, F., Bolton, S., Connerney, J. E. P., et al. (2017). Hot flow anomaly observed at Jupiter's bow shock. *Geophysical Research Letters*, 44, 8107–8112. <https://doi.org/10.1002/2017GL073175>
- Vogt, M. F., Bunce, E. J., Kivelson, M. G., Khurana, K. K., Walker, R. J., Radioti, A., et al. (2015). Magnetosphere-ionosphere mapping at Jupiter: Quantifying the effects of using different internal field models. *Journal of Geophysical Research: Space Physics*, 120, 2584–2599. <https://doi.org/10.1002/2014JA020729>
- Williams, D. J., Mauk, B. H., McEntire, R. E., Roelof, E. C., Armstrong, T. P., Wilken, B., et al. (1996). Electron beams and ion composition at Io and in its torus. *Science*, 274(5286), 401–403. <https://doi.org/10.1126/science.274.5286.491>
- Williams, D. J., & Thorne, R. M. (2003). Energetic particles over Io's polar caps. *Journal of Geophysical Research*, 108(A11), 1397. <https://doi.org/10.1029/2003JA009980>
- Zarka, P. (1998). Auroral radio emissions at the outer planets: Observations and theories. *Journal of Geophysical Research*, 103, 20,159–20,194. <https://doi.org/10.1029/98JE01323>